ARTICLE   OPEN

Lifespan-increasing drug nordihydroguaiaretic acid inhibits p300 and activates autophagy

Tugsan Tezil [ID][1], Manish Chamoli [ID][1], Che-Ping Ng[1], Roman P. Simon[2], Victoria J. Butler[3], Manfred Jung [ID][2], Julie Andersen[1], Aimee W. Kao [ID][3] and Eric Verdin [ID][1]*

Aging is characterized by the progressive loss of physiological function in all organisms. Remarkably, the aging process can be modulated by environmental modifications, including diet and small molecules. The natural compound nordihydroguaiaretic acid (NDGA) robustly increases lifespan in flies and mice, but its mechanism of action remains unclear. Here, we report that NDGA is an inhibitor of the epigenetic regulator p300. We find that NDGA inhibits p300 acetyltransferase activity in vitro and suppresses acetylation of a key p300 target in histones (i.e., H3K27) in cells. We use the cellular thermal shift assay to uniquely demonstrate NDGA binding to p300 in cells. Finally, in agreement with recent findings indicating that p300 is a potent blocker of autophagy, we show that NDGA treatment induces autophagy. These findings identify p300 as a target of NDGA and provide mechanistic insight into its role in longevity.

INTRODUCTION

Aging is associated with an increase in age-related diseases that include many cancers, neurodegenerative diseases (e.g., Parkinson's and Alzheimer's), atherosclerosis and associated cardiovascular disorders (e.g., heart attacks and stroke), macular degeneration, osteoarthritis, and sarcopenia.[1] Remarkably, aging or its manifestations as chronic diseases of aging can be slowed by a number of interventions that include diet, exercise, and pharmaceutical drugs.[2] The Interventions Testing Program at the National Institute on Aging has tested 27 drugs for their effects on lifespan in mice. They identified six drugs, including rapamycin, aspirin, acarbose, nordihydroguaiaretic acid (NDGA), protandim, and 17α-estradiol, that were associated with increased median lifespan.[3–6] In particular, NDGA showed a consistent median lifespan extension by 8–10% at three different doses in mice, particularly in males. Old mice (22 months old) treated with NDGA showed improved grip duration and rotarod performance, indicating better muscle function than untreated age-matched animals. NDGA also extends median lifespan in evolutionarily distant organisms, such as fruit flies (by 12%) and mosquitoes (by 50%).[7,8] Several studies also showed the effects of NDGA on neurodegenerative disorders. In a fruit fly model of Parkinson's disease, NDGA delayed the loss of climbing ability associated with onset of neurodegeneration.[9] NDGA also decreased motor dysfunction in a mouse model of amyotrophic lateral sclerosis and extended lifespan by 10% in this context.[10] Furthermore, NDGA restored synapse structure and extended lifespan by 19% in a mouse model of Huntington's disease[11] and decreased amyloid-beta deposition in the brains of mouse models of Alzheimer's disease.[12,13]

In vitro studies show that NDGA scavenges hydroxyl radical, peroxynitrite, superoxide anion and singlet oxygen, suggesting that NDGA might function as an antioxidant agent.[14,15] In vivo, NDGA exerts cytoprotective effects by modulating the nuclear factor erythroid 2-related factor 2 (Nrf2)/antioxidant response element (ARE) antioxidant pathway.[16] This variety of effects makes NDGA a compelling candidate for further study in the context of aging and geroprotective processes.

The hallmarks of aging include epigenetic alterations and deregulation of nutrient sensing.[1] Levels of histone acetylation change during aging and are related to increased acetyl-CoA levels in aging animals,[17] and acetyl-CoA levels decrease significantly upon calorie restriction even before cellular ATP, NADH, or amino acid levels are affected.[18,19] As acetyl-CoA is the only acetyl-group donor for protein acetylation reactions, its cellular level highly influences the activity of acetyltransferases.[20] Particularly, histone and nonhistone acetyltransferase p300 (E1A-associated protein p300) functions as a molecular sensor of changes in cellular and possibly other acyl-CoA levels as well.[21] Any decrease in cellular acetyl-CoA significantly limits the activity of p300 and decreases subsequent acetylation reactions involving key cellular proteins.[22,23] Notably, p300 potently blocks autophagy by acetylating autophagy-related proteins including Atg5, Atg7, Atg12, and LC3.[24]

Although the health benefits of NDGA have been demonstrated in different organisms and conditions, its underlying mechanism of action remains unclear. Early reports show that NDGA inhibits arachidonic acid 5-lipoxygenase,[25] which catalyzes the first step in leukotriene A4 biosynthesis, and lysophosphatidylcholine acyltransferase-2 (LPCAT2),[26] an enzyme in platelet-activating factor (PAF) biosynthesis that converts the precursor lyso-PAF (1-O-alkyl-sn-glycero-3-phosphocholine) into active PAF (1-O-alkyl-2-acetyl-sn-glycero-3-phosphocholine) by acetylation. Interestingly, salicylate (an active metabolite of aspirin) and diflunisal (a salicylate derivative) both also inhibit LPCAT2.[27]

We recently reported that both salicylate and diflunisal are inhibitors of the histone acetyltransferase p300.[28] Here we tested the possibility that NDGA also inhibits p300 and exerts its effect on aging by inhibition of this important epigenetic regulator. We report that NDGA inhibits p300. We further present evidence of NDGA directly binding to p300 in cells and show that NDGA

[1]Buck Institute for Research on Aging, 8001 Redwood Boulevard, Novato, CA 94945-1400, USA. [2]Institute of Pharmaceutical Sciences, University of Freiburg, Albertstrasse 25, Freiburg 79104, Germany. [3]Department of Neurology, University of California, San Francisco, CA 94143, USA. *email: everdin@buckinstitute.org

treatment activates the autophagy pathway and promotes autophagosome formation in human cells, as well as in *C. elegans*.

RESULTS

NDGA inhibits p300 in vitro

To test the hypothesis that NDGA is a p300 inhibitor, we used two different in vitro enzymatic assays that measure the acetyltransferase activities of p300 and PCAF (p300/CBP-associated factor). In the first assay, we used purified human recombinant p300 BHC protein[29] (a construct containing the bromodomain, catalytic acetyltransferase domain, and C/H3 domain, amino acids 965–1810) that represents the acetyltransferase activity of full length protein,[30] histone H3 (amino acids 1–21) peptide as a substrate, and acetyl-CoA as an acetyl-group donor, to measure the activity of p300 on histone H3 in the presence of NDGA. In this fluorimetric assay, NDGA inhibited p300 BHC with an IC_{50} of 10.3 μM, compared with 75 μM for the known p300 inhibitor anacardic acid[31] (Fig. 1a). When we evaluated NDGA for the

inhibition of human recombinant PCAF HAT (histone acetyltransferase domain), we observed no inhibition even at high concentrations of NDGA (Fig. 1b), ruling out a nonspecific mechanism of action. In the second assay, we used purified human recombinant p300 HAT protein consisting of the core HAT only (amino acids 1284–1673), histone H3 peptide (amino acids 1–21), and acetyl–CoA mixture in reaction buffer containing increasing concentrations of NDGA. Consistent with Fig. 1a, b, NDGA inhibited p300 HAT activity (Fig. 1c) but failed to inhibit purified human PCAF HAT activity (Fig. 1d). To further understand the mechanism of p300 inhibition, we determined inhibition kinetics of p300 HAT activity by NDGA for both substrates acetyl-CoA and H3 peptide. Double-reciprocal plots were constructed to find the nature of inhibition. Inhibition kinetics studies clearly showed that NDGA is a noncompetitive inhibitor for both acetyl-CoA (Fig. 1e) and histone H3 binding sites (Fig. 1f). These results indicate that NDGA is a selective inhibitor of p300 acetyltransferase activity in vitro.

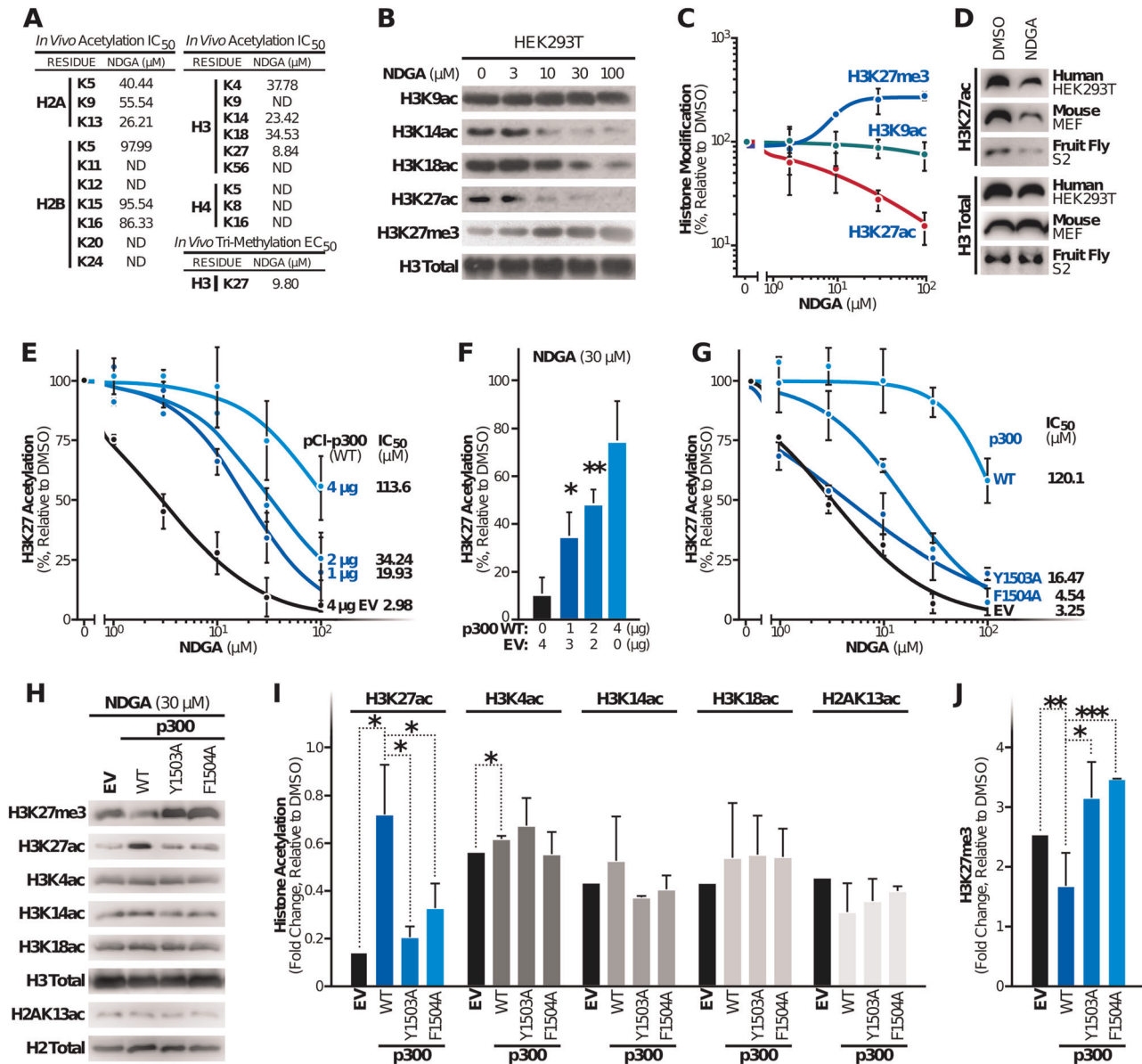### NDGA inhibits p300-mediated histone acetylation in human, mouse and fruit fly cells

As an epigenetic regulator, p300 orchestrates gene expression via acetylation of specific lysine residues in specific cellular histone proteins in cells.[32] To determine whether NDGA influences histone acetyl marks in cells, we monitored the acetylation status of different lysine residues in HEK293T cells treated with NDGA. Specifically, we extracted the histones and conducted western blot analysis using antibodies selective for unique acetylated histone residues and determined IC_{50} values for each residue (Fig. 2a, Supplementary Fig. 1). Previous genetic studies reported that deletion of p300 specifically reduces acetylation on H3K27 but not H3K9.[33] Consistent with our hypothesis that NDGA selectively inhibits p300 in cells, we found that histone H3K27 acetylation was the most suppressed in cells treated with NDGA with an IC_{50} of 8.8 μM (Fig. 2a–c). The acetylation of other histone residues was also suppressed but in most cases with $IC_{50} > 25$ μM, except for H3K14 (Fig. 2a). As expected, residues that are not p300 targets, such as H3K9, were unchanged by NDGA (Fig. 2a–c).

To test the effect of NDGA on H3K27 acetylation in different organisms, we also treated mouse (MEF) and fruit fly (S2 Schneider) cell lines with NDGA (30 μM) for 24 h, and analyzed extracted histones by immunoblotting. As with HEK293T, H3K27 acetylation was also found to be decreased also in these cell lines upon NDGA treatment (Fig. 2d, Supplementary Fig. 2), demonstrating the suppressive effect of NDGA on H3K27 acetylation in evolutionarily distant organisms.

NDGA-induced suppression of H3K27ac is associated with increased tri-methylation of the same residue in HEK293T cells

Decreased histone H3 K27 tri-methylation (H3K27me3) is a characteristic hallmark of aging in both invertebrates and vertebrates. Worms and fruit flies exhibit an age-associated decrease in H3K27me3 marks,[34] but in humans, a strong decrease in this modification has been observed in primary fibroblasts from patients with Hutchinson–Gilford progeria syndrome, a premature aging disease.[35] Conversely, the naked mole rat, which is the longest-living rodent with a lifespan of more than 28 years,[36] bears higher levels of H3K27 tri-methylation compared to mice.[37] Since acetylation and methylation are mutually exclusive on a single lysine, decreased acetylation can result in an increase in methylation on the same residue.[38] Therefore, we treated HEK293T cells with increasing concentrations of NDGA, extracted histones, and determined the methylation status of H3K27 by immunoblotting. As predicted and in agreement with the decrease in H3K27 acetylation, cells treated with NDGA showed a significant increase in H3K27 tri-methylation with a half maximal effective concentration (EC_{50}) of 9.80 μM (Fig. 2a–c).
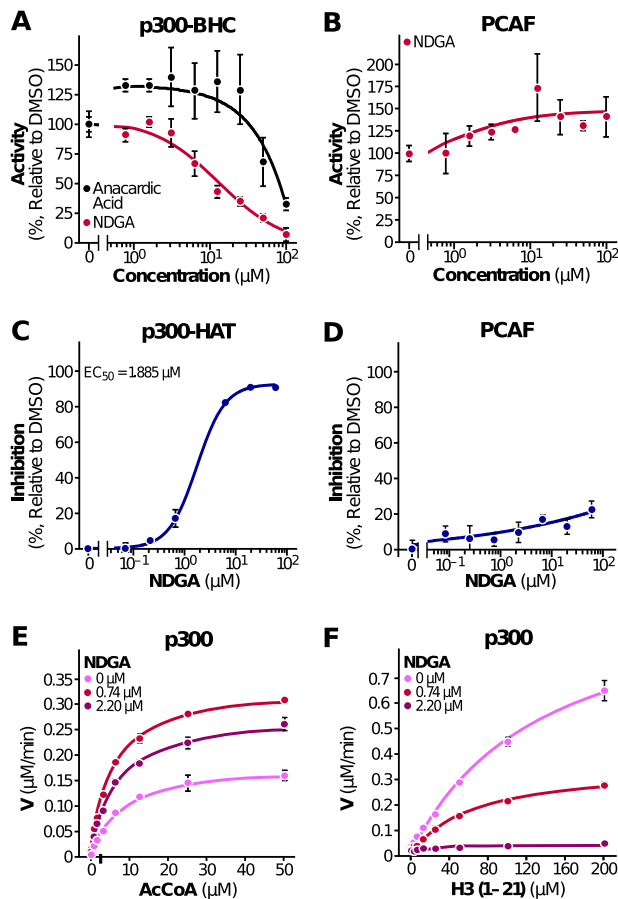
Fig. 1 NDGA inhibits histone acetyltransferase activity of p300 in vitro. **a** The acetyltransferase activity of p300 on histone H3 peptide (aa 1–21) was measured in the presence of NDGA or anacardic acid. Results are expressed as percentage activity in the absence of NDGA. A paired *t*-test was performed for statistical significance, $p = 0.0013$. **b** Effect of NDGA on PCAF HAT activity expressed as percentage activity in the absence of NDGA. Inhibitory effects of NDGA on p300 (**c**) and PCAF (**d**) using another enzymatic assay were measured and are expressed as percentage inhibition relative to control DMSO. Effects of varying concentrations of acetyl-CoA (**e**) and substrate peptide histone H3 in the presence of varying concentrations of NDGA were measured (**f**). Data represent the results from three independent experiments (mean ± S.D.), and curves were generated using nonlinear regression fit

Fig. 2 NDGA inhibits p300-driven histone acetylation in HEK293T cells. **a** Median inhibitory concentration (IC_{50}) values for NDGA on different acetylated histone residues and median effective concentration (EC_{50}) value on H3K27 tri-methylation were determined by immunoblotting of histones extracted from cells after 24-h treatments with varying concentrations of NDGA (ND, not determined). **b** Differences in acetylation and tri-methylation of p300 target (H3K14, H3K18, and H3K27) and non-target (H3K9) histones were monitored by immunoblotting after indicated concentrations of NDGA treatment for 24 h and histone extraction. **c** Dose-dependent changes in acetylation and tri-methylation on H3K27 after 24-h NDGA treatment were analyzed by immunoblotting and are represented as percentage change in histone modification relative to DMSO treatment. **d** Decreases in H3K27 acetylation upon 30 μM of NDGA treatment for 24 h in human (HEK293T), mouse (MEF) and fruit fly (S2 Schneider) cells were monitored by immunoblotting after histone extraction. **e**. Effects of wildtype p300 overexpression on NDGA-dependent H3K27 hypoacetylation were determined by densitometric analysis of immunoblotting data. Cells were transfected with different amounts of human wildtype EP300 encoding expression plasmid pCI-p300(WT) and/or empty vector (EV) and treated with varying NDGA concentrations for 24 h. The data represent percentage change in H3K27 acetylation relative to DMSO treatment and the change in IC_{50} values. **f** The rescue of p300 overexpression on H3K27 hypoacetylation after 30 μM NDGA treatment was performed as in panel E. **g** Effects of overexpression of wildtype and catalytically inactive p300 mutants (Y1503A and F1504A) on NDGA-induced H3K27 hypoacetylation were determined by immunoblotting and densitometry. Cells were transfected by the same amount of expression plasmids or empty vector (EV) and treated with varying NDGA concentrations. Histones were extracted and analyzed. **h** The effects of wildtype and mutant (Y1503A or F1504A) p300 overexpression on NDGA-induced histone hypoacetylation and hypermethylation were determined by immunoblotting after 30 μM NDGA treatment for 24 h. **i** Effects of wildtype and mutant p300 overexpression on NDGA-induced histone hypoacetylation were analyzed by immunoblotting and densitometry. **j** Decreased H3K27 tri-methylation upon wildtype p300 overexpression was detected by immunoblotting and densitometry. Total histone antibodies were used as loading controls in all experiments. Data represent the results from two independent experiments (mean ± S.D.) and curves were generated using nonlinear regression fit
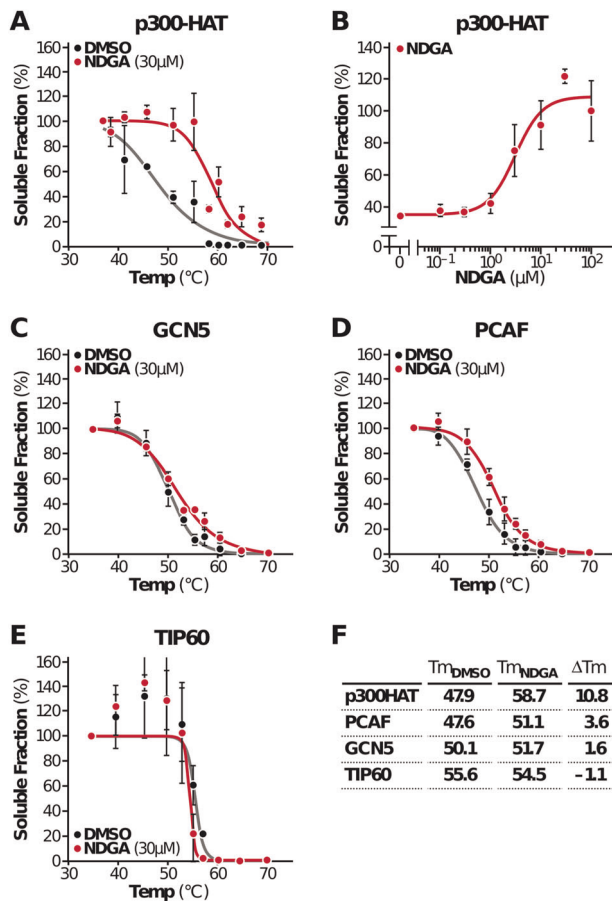
Fig. 3 NDGA is a target of NDGA in HEK293T cells. **a** Melting curves of the p300 HAT domain were generated from a CETSA experiment performed in intact cells expressing HA tagged p300-HAT construct following 3-h DMSO or NDGA treatment. **b** Isothermal dose-response fingerprint-CETSA (ITDRF$_{CETSA}$) graph was generated from cells expressing the p300-HAT construct. Intact cells were treated with different concentrations of NDGA for 3 h and subjected to heating at 55 °C for 3 min to monitor thermostabilization. Melting curves of different acetyltransferases were generated from intact cells expressing HA-GCN5 (**c**), HA-PCAF (**d**) or HA-TIP60 (**e**) after 3-h DMSO or 30 μM NDGA treatment and CETSA. **f** Change in melting temperatures (T_m) of tested proteins upon NDGA treatment. Data represent the results from two independent experiments (mean ± S.D.), and curves were generated using nonlinear regression fit

Overexpression of p300 reverses NDGA-induced loss of H3K27 acetylation

To further assess p300 as a relevant target of NDGA, we overexpressed different amounts of full-length p300 in HEK293T cells and treated them with NDGA. In support of a role for p300 in sustaining H3K27 acetylation, we found that over-expression of p300 suppressed the effect of NDGA in a dose-dependent manner and increased H3K27 acetylation (Fig. 2e, Supplementary Fig. 3). The IC$_{50}$ of NDGA in rescue experiments was strongly correlated with the amount of p300-expressing plasmid transfected (Fig. 2f, Supplementary Table 1). Furthermore, addition of catalytically inactive p300 mutants (p300Y1503A and F1504A)[39] failed to revert NDGA-mediated inhibition (Fig. 2g, Supplementary Fig. 3). In addition to H3K27 acetylation, we also evaluated the acetylation of other histone residues with an IC$_{50}$ lower than 50 μM (H3K4, H3K14, H3K18, H2AK13). While we observed a significant rescue effect on H3K27 and a slight rescue in H3K4 acetylation with wildtype p300 overexpression, changes in other acetylated residues were insignificant (Fig. 2h, i,

Supplementary Fig. 4). In agreement with our previous result, we observed a significant decrease in H3K27 tri-methylation when wildtype p300 was overexpressed; whereas overexpression of mutant p300 was unable to change the levels of H3K27me3 (Fig. 2j, Supplementary Fig. 4). These findings support the hypothesis that NDGA-mediated H3K27 hypoacetylation and elevated H3K27 tri-methylation are specifically due to inhibition of p300 acetyltransferase activity.

p300 is a direct target of NDGA in HEK293T cells

To provide additional evidence that NDGA directly binds to p300 in cells, we used a cellular thermal shift assay (CETSA) that uniquely allows monitoring of drug engagement inside cells.[40] Based on the principle of ligand-induced protein stabilization, compound-bound proteins precipitate at higher temperatures than unbound proteins and can be detected at higher levels in the soluble fraction. To identify direct targets of NDGA, we tested different acetyltransferases. We exogenously expressed p300 HAT (p300/CBP family), GCN5 (general control of amino acid synthesis protein 5-like 2) and PCAF (GNAT family), and TIP60 (60-kDa Tat-interactive protein, MYST family) in HEK293T cells and treated the cells with NDGA. Intact cells were heated at different temperatures for 3 min to denature and precipitate proteins. These cells were then subjected to three freeze-thaw cycles to lyse them, isolation of a soluble fraction after centrifugation (20,000 × g) and analysis by immunoblotting. We observed an increase in the thermo-stability of p300 HAT domain by 10.8 °C upon NDGA treatment (Fig. 3a, Supplementary Fig. 5). To confirm this thermostabilization in a dose-dependent manner, we treated cells with different concentrations of NDGA and heated them at a single temperature (55 °C) where we previously detected 35% of the total amount of p300 in the soluble fraction. Maximal stabilization (100%) occurred at 30 μM NDGA (Fig. 3b, Supplementary Fig. 5). Importantly, CETSA analysis of GCN5, PCAF, and TIP6 (Fig. 3c–e, Supplementary Fig. 5) showed no significant change in thermostability upon NDGA treatment. The difference in melting temperatures (T_m) of proteins tested are shown in Fig. 3f. These results further support the model that NDGA specifically binds to p300 HAT at a concentration consistent with its inhibitory activity on histone acetylation (Fig. 2).

NDGA induces autophagy in HEK293T and HeLa cells

While we demonstrated a potential molecular mechanism for the role of NDGA in aging cells above, the cellular mechanism by which NDGA elicits these effects remains unexplored. p300, the molecular target of NDGA, is a regulator of cellular autophagy, an evolutionarily conserved process for efficient removal of damaged and potentially harmful cellular contents, including long-lived proteins and cellular organelles.[41] To accomplish this cellular cleansing effort, the coordinated actions of various autophagy-related (Atg) proteins are required. Atg proteins provide the main molecular machinery essential for initiating autophagosome formation via an ubiquitin-like conjugation system.[42] Interestingly, p300 modulates the acetylation status of several Atg proteins. Silencing of p300 expression reduces the acetylation of Atg5, Atg7, LC3, and Atg12, and increases their stability and cellular level, resulting in autophagy pathway activation. Overexpression of p300, on the other hand, causes a significant increase in acetylation, decreases the stability of mentioned key proteins, and consequently blocks autophagy by lowering their cellular level. These previous results predict that inhibiting p300 by NDGA could act through activating autophagy. To test this hypothesis, we measured the level of autophagy after NDGA treatment and in response to serum-free media as a positive control. Adding NDGA to HEK293T cells induced several molecular markers of autophagy, including AMPK phospho-activation and upregulation of Beclin-1 (Fig. 4a, Supplementary Fig. 6).
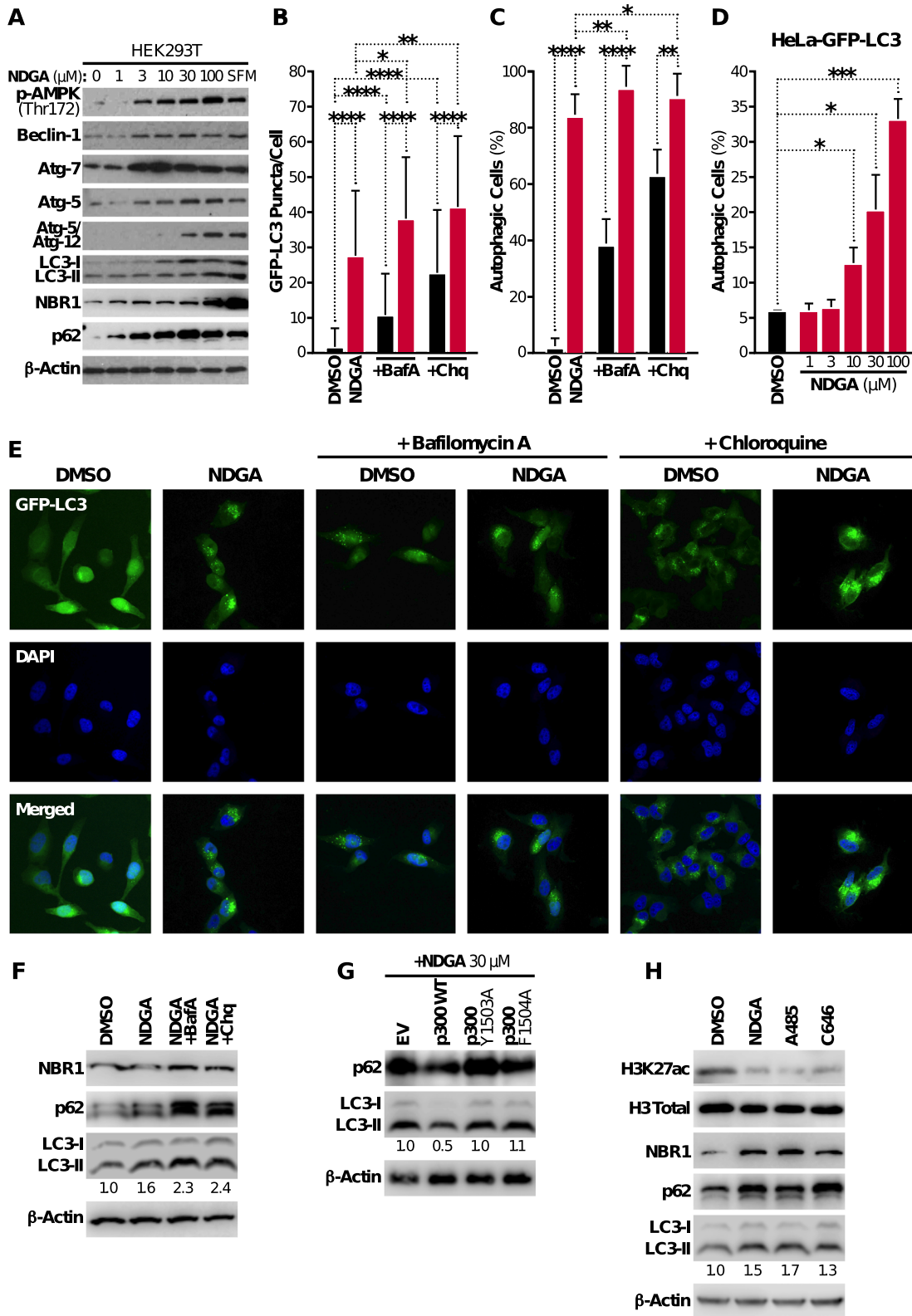
Atg proteins together regulate the formation of a double membrane structure (autophagosome) that engulfs the cellular cargo targeted for degradation.[43] Briefly, Atg7 induces Atg12-Atg5 conjugation and this conjugate specifies localization of LC3 on the lipid membrane. Our results showed a dose-dependent increase in Atg7 levels, and an increase in Atg5/Atg12 dimerization (Fig. 4a,

Supplementary Fig. 6), consistent with induction of autophagy. In addition, we observed upregulation of LC3-II, which is associated with autophagosome formation as well as upregulation of the autophagy cargo receptors NBR1 (Neighbor of BRCA1 gene 1) and p62 (SQSTM1, Sequestosome-1) upon treatment with NDGA (Fig. 4a, Supplementary Fig. 6). To confirm the induction of autophagy

Fig. 4 NDGA induces autophagy in HEK293T and HeLa cells. **a** Activation of the autophagy signaling pathway was monitored by immunoblotting of total proteins isolated from HEK293T cells after a 24-hour treatment with DMSO or varying concentrations of NDGA. Serum-free medium (SFM) was used as a positive control of autophagy. **b** Autophagosome formation in HeLa-GFP-LC3 cells was monitored by counting GFP-LC3 puncta after a 24-h treatment with DMSO or NDGA, with or without Bafilomycin A1 (BafA, 100 nM) or Chloroquine (Chq, 100 μM) treatment 3 h before sample collection. **c** The percentage of autophagy was measured in HeLa-GFP-LC3 cells treated with DMSO or NDGA, with or without Bafilomycin A1 or Chloroquine treatment for 3 h prior to sample collection. The threshold value to determine autophagy-positive cells was based on previous measurements and DMSO-treated cells; d. Autophagy induction in HeLa-GFP-LC3 cells was analyzed by FACS after a 24-h treatment with varying NDGA concentrations. **e** GFP-LC3 puncta (green) in HeLa-GFP-LC3 cells treated with DMSO or NDGA, with or without Bafilomycin A1 or Chloroquine were captured by confocal microscopy. Cells were fixed after 24-h treatment, stained with DAPI (blue) and analyzed. **f** Effects of Bafilomycin A and Chloroquine treatment for 3 h on autophagy marker proteins were quantitated by immunoblotting following total protein extraction. **g** Effects of wildtype and mutant (Y1503A and F1504A) p300 overexpression on NDGA-induced autophagy were monitored by immunoblotting. **h** Effects of p300 inhibitors on H3K27 acetylation and autophagy induction were analyzed by immunoblotting. HEK293T cells treated with NDGA (100 μM), A485 (100 nM) or C646 (100 μM) for 24 h, and total protein or histones were extracted. Numbers in immunoblotting images (**f**–**h**) indicate the fold change determined by densitometry analysis. β-Actin and total histone H3 were used as loading controls. Data represent the results from two independent experiments (mean ± S.D.), and statistical significance was determined by student t-test (*$p < 0.05$; **$p < 0.01$, ***$p < 0.001$, ****$p < 0.0001$)

in cells, we visualized the process by imaging HeLa cells stably expressing GFP-LC3. Following a 24-h treatment with NDGA (30 μM) or DMSO, we analyzed LC3 lipidation. LC3-positive puncta were significantly increased with NDGA treatment. Moreover, treatment with Bafilomycin A1, an V-ATPase inhibitor that prevents the fusion of autophagosomes and lysosomes,[44] or with the lysosomal pH-neutralizing compound Chloroquine[45] resulted in an additional increase in GFP-LC3 puncta in treated cells (Fig. 4b, e). These results indicate the accumulation of autophagosomes demonstrating that HeLa-GFP-LC3 cells have a functional autophagy pathway. An increase in autophagosome number upon NDGA treatment caused a rise in the number of cells undergoing autophagy (Fig. 4c, e). We also observed that the pro-autophagic effect of NDGA was dose-dependent (Fig. 4d, Supplementary Fig. 7). NDGA-treated HEK293T cells showed increased levels of endogenous NBR1, p62, and LC3-II upon NDGA treatment; Bafilomycin A or Chloroquine treatment further enhanced this effect (Fig. 4f, Supplementary Fig. 6). Since the overexpression of p300 rescues H3K27 hypoacetylation (Fig. 2f), we next evaluated p62 and LC3-II levels in wildtype versus mutant p300 over-expressing HEK293T cells upon NDGA treatment. Figure 4g shows the rescue effect of excess p300 expression by downregulation of these autophagy markers (Supplementary Fig. 6). When we compared NDGA with other p300 inhibitors C646 and A485 for autophagy induction, we discovered that these inhibitors also increased the levels of autophagy markers NBR1, p62, and LC3-II in HEK293T cells (Fig. 4h, Supplementary Fig. 6). These data indicate that NDGA effectively increases autophagic flux in HEK293T and GFP-LC3 HeLa cells, and that p300 activity is a key element in NDGA-induced autophagy.

NDGA increases median lifespan, decreases histone acetylation, and induces autophagy in worms

To determine the prolongevity property of NDGA in vivo, we treated wildtype *C. elegans* (N2 Bristol) with 100 μM NDGA. The median lifespan of worms exposed to NDGA was 21.4% greater than that of worms exposed to the vehicle alone (DMSO) (Fig. 5a). To rule out potential variations in food availability caused by NDGA, we examined the effect of NDGA on feeding bacteria (OP50) and found that OP50 growth was unaffected by NDGA (Fig. 5b). These findings indicate that NDGA has a beneficial effect on *C. elegans* lifespan that is independent of the feeding bacteria growth.

CBP-1, the nematode orthologue of p300/CBP, is responsible for histone acetylation in *C. elegans*, and animals with catalytically inactive cbp-1 have decreased global histone acetylation.[46] With this knowledge, we evaluated the possible suppressive effect of NDGA on histone H3 acetylation. We treated worms with 100 μM NDGA for 24 h, analyzed histone H3 acetylation by

immunoblotting and observed a significant decrease in histone H3 acetylation in treated animals (Fig. 5c, d, Supplementary Fig. 8).

To analyze autophagy induction in worms in depth, we used described reporter strain (MAH215) expressing pH sensitive GFP in a tandem *lgg-1p::mCherry::GFP::lgg-1* in which mCherry puncta indicates autophagosomes and autolysosomes.[47] Worms exposed to NDGA had an increase in mCherry-only puncta, indicating an elevated autophagic activity as assessed by increased fusion of autophagosomes to lysosomes (Fig. 5e, g). MAH215 worms with this tandem reporter allow us to analyze the autophagosome maturation process by monitoring the GFP and mCherry fluorescence intensity over time. Increased autophagic flux and lysosomal activity following NDGA treatment is also evident from observed decreases in pH-sensitive GFP fluorescence over time resulting from the quenching of GFP within the acidic lysosome. We examined the NDGA-treated worms (2–24 h) by measuring the ratio of GFP relative to mCherry fluorescence. We observed that GFP signal was significantly less in animals treated for 2 h than in the vehicle-treated animals (DMSO), and those levels continued to decrease at 24 h (Fig. 5f). In agreement with these results, worms treated with NDGA also show increased lysotracker staining, suggesting an increased number of lysosomes/late endosomes most likely as a result of increased autophagic activity (Fig. 5h, i). These data provide evidence that NDGA treatment causes an increase in autophagic flux in *C. elegans*.

DISCUSSION

Here we present evidence for a potential mechanism for NDGA actions as a lifespan increasing drug. We showed that NDGA effectively inhibits p300 histone acetyltransferase activity in vitro, and it directly binds the p300 HAT domain and alters several epigenetic marks associated with aging in human, mouse, and fruit fly cells. Notably, while we identify p300 as a target of NDGA, we cannot exclude the possibility that it blocks the activity of other acetyltransferases. For example, CREBBP (CBP), which shares high levels of homology with the p300 catalytic domain, is likely to be also targeted by NDGA. But importantly, NDGA failed to enhance the thermostability of GNAT family members PCAF and GCN5 and the MYST family member TIP60 in CETSA experiments.

p300/CBP is conserved in different organisms from nematodes to mammals and plays an essential role in cell and organism viability. Worms with inactive CBP-1, knockout of dCBP (the fruit fly homolog of p300/CBP), and homozygous p300 or CBP knockout mice demonstrate embryonic lethal phenotypes.[48,49] These observations indicate that the use of potent pharmacologic inhibitors of p300 in clinic might cause unintended toxicity in younger animals. Therefore, p300 inhibition may be more applicable during late adulthood or for the treatment of age-related diseases that rely on elevated p300 activity such as cancer
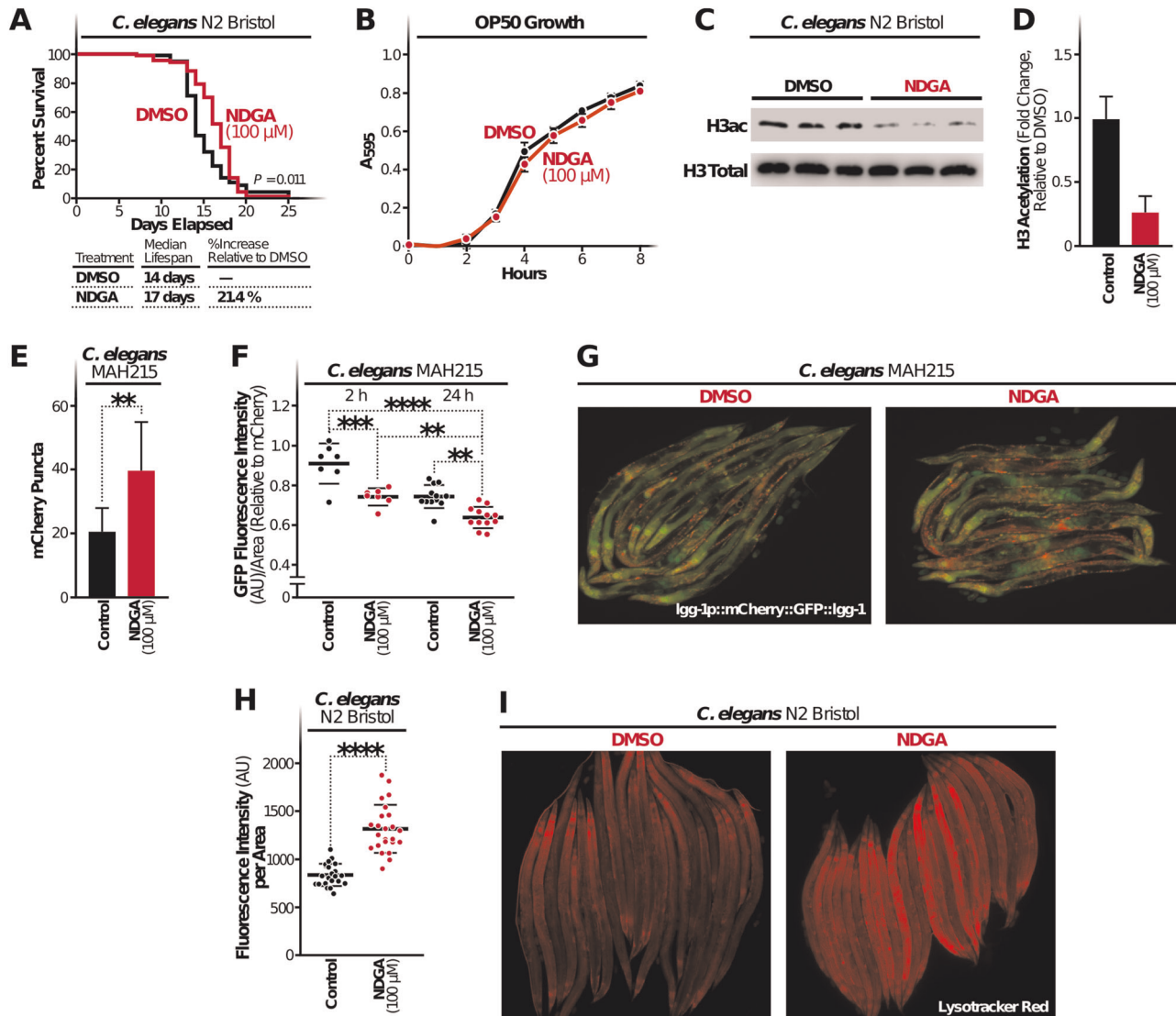
Fig. 5 NDGA increases median lifespan and induces autophagy in worms. **a** The effect of NDGA on worm lifespan was measured by exposing N2 worms to DMSO or NDGA (100 μM) on NGM plates. Average values from three independent experiments were plotted as a lifespan curve. Lower panel indicates the median lifespan of each group as days and percentage; **b** The effect of NDGA on feeding bacteria (*E. coli* OP50) growth was measured spectrophotometrically (A_{595}) every hour for 8 h in LB medium with 100 μM of NDGA or DMSO. **c, d** Total histone H3 acetylation in worms was measured by immunoblotting after 24-h NDGA (100 μM) or DMSO exposure and total protein extraction. **e** Changes in mCherry puncta number in MAH215 worms were monitored by fluorescence microscopy after a 24-h NDGA or DMSO treatment. **f** Effects of NDGA treatment on GFP by time were measured by fluorescence microscopy after NDGA or DMSO (Control) treatment for 2 and 24 h and represented relative to mCherry intensity. **g** Monitoring of tandem reporter *lgg-1p::mCherry::GFP::lgg-1* expressing worms was performed by fluorescence microscopy. **h, i** Monitoring Lysotracker Red staining in N2 worms after 24-h treatment with NDGA (100 μM) or DMSO was performed by fluorescence microscopy, and fluorescence intensity was measured for individual animals in each group. Data represent the results from three independent experiments (mean ± S.D.), and statistical significance was determined by student *t*-test (*$p < 0.05$; **$p < 0.01$, ***$p < 0.001$)

and neurodegenerative diseases.[50,51] Several chemical inhibitors with varying potency and selectivity for p300 have already been tested for their potential anticancer properties, including anacardic acid,[52] C646,[53] and A485.[54]

Previous studies on NDGA carried out with mice fed diets containing different doses of NDGA have determined that blood levels of NDGA in supplemented animals (165 nM) are lower than those we found to be required to inhibit p300 in cell-free systems and to activate autophagy in cells. However, it should be noted that tissue and plasma concentrations of a compound are not linearly correlated factors. In fact, several studies previously reported this phenomenon.[55,56] The concentration of NDGA in serum, uptake in different tissues and its intracellular

concentration may vary. Currently, it is unknown how NDGA is metabolized, which proteins are involved in its cellular uptake in different tissues, and how NDGA is distributed in the body. These characteristics of NDGA should be further investigated in different cells and tissues.

Previous studies on mice indicate a sexual dimorphism in response to NDGA treatment: males showed an increase in median lifespan, but females did not. Importantly, this study also showed that the median lifespan of control female mice is ~10% higher than males, and that NDGA-treated males demonstrate a level of benefit similar to the control lifespan curves of females. Therefore, NDGA may provide beneficial effects in both females and males, but possible adverse effects in females could prevent

lifespan extension. Moreover, several compounds extend lifespan differently favoring either sex. For instance, acarbose and 17-α estradiol show either smaller or no lifespan extension in female mice, compared to males. Aspirin and rapamycin inhibit inflammatory response, which could have a sex-dependent effect in late-life inflammation.[57] Sex difference in autophagy induction has also been documented and may influence the efficacy of a compound.[58] The dimorphic nature in response to NDGA or other lifespan-extending compounds still needs to be understood with further studies.

Activation of autophagy has emerged as an important intervention against aging and the chronic diseases of aging, and its inhibition reverses the beneficial effects of anti-aging interventions in all species investigated to date.[59] Importantly, p300 decreases the stability of Atg5, Atg7, Atg12, and LC3 by acetylation and functions as an anti-autophagic regulator under high nutrient conditions. Our findings are in accord with several reports showing autophagy induction upon inhibition of p300.[60] Our results highlight the role of p300 and pharmacological inhibitors, such as NDGA, in key aging-related molecular and cellular processes. These observations support the hypothesis that the suppressor function of p300 on autophagy can also be regulated pharmacologically.

Moreover, other interventions that increase lifespan, such as spermidine, aspirin, calorie restriction, and rapamycin, also provide their beneficial effects in part by inducing autophagy, potentially through p300 inhibition.[61–64] While spermidine and aspirin directly inhibit p300, calorie restriction diminishes p300 activity indirectly by lowering cellular acetyl-CoA levels.[65] Rapamycin indirectly inhibits p300 by suppressing mTORC1, which phosphorylates p300 and prevents its intramolecular inhibition, resulting in autophagy suppression.[66] Together with our results, these findings underscore the significant role of p300 in aging and could generate renewed interest in evaluating the clinical utility of p300 inhibitors for both aging and age-related diseases.

METHODS

Cell culture
HEK293 (ATCC), HeLa-LC3-GFP, and MEF (ATCC) cells were maintained in appropriate volume of Dulbecco's Modified Eagle Medium supplemented with 10% serum (Serum Plus - II, Sigma), 100 units/mL penicillin and 100 units/mL streptomycin (Corning, VA). Schneider's Drosophila Line 2 (S2 Schneider) was kindly provided by Henri Jasper, Buck Institute for Research for Aging. S2 cells were grown at 25 °C in Schneider's Insect Medium (Himedia) that was prepared according to the manufacturer's instructions.

Chemicals and buffers
NDGA (Sigma), C646 (Sigma), A485 (Tocris), and Bafilomycin A1 (Adipogen) were dissolved in dimethyl sulfoxide (DMSO) (Sigma-Aldrich), Chloroquine (Biovision) was dissolved in water. Phosphate-buffered saline (PBS) was purchased from Corning. Tris-buffered saline with Tween (TBST) buffer (150 mM NaCl, 0.01% (v/v) Tween-20, 50 mM Tris-HCl buffer, pH 7.6) was used for immunoblotting. Blocking buffer and primary antibody incubation solution was 5% (w/v) BSA (Sigma), pH 7.0, in TBST. Secondary antibody incubation buffer was 5% (w/v) blocking reagent (Sigma) in TBST.

Plasmids and transfection
HEK293T cells were transfected using TransIT-X2 (Mirus) reagent, following the manufacturer's instructions, and further treatments were carried out 48 h post transfection. Full-length wildtype p300, p300(Y1503A), and p300 (F1504A) were used for rescue experiments. Primers used for cloning are listed in Supplementary Notes.

In vitro acetyltransferase activity assays
The activities of histone acetyltransferases, p300 and PCAF, were measured using a fluorimetric assay kit, following the manufacturer's instructions (SensoLyte p300 Assay kit, SensoLyte PCAF Assay kit, Anaspec) using appropriate dilutions of NDGA and anacardic acid. To measure the inhibition of p300 and PCAF, appropriate dilutions of NDGA and anacardic acid were prepared and added to the assay mixture. The manual in vitro acetyltransferase assay kit was performed in reaction buffer (final concentration; 40 mM HEPES pH 7.5, 40 mM NaCl, 0.025% Triton X-100, 50 μM histone H3 peptide (amino acids 1–21), 40 nM p300 (Enzo Life Science, BML-SE451), or 30 nM PCAF (Cayman Chemical, 10009115)) in black 96-well microtiter plates (PerkinElmer, 6005320). Appropriate dilutions of NDGA were prepared and added to the assay mixture. Enzyme concentrations were evaluated to give a linear response between enzyme concentration and initial velocity for each acetyltransferase tested. Negative controls received assay buffer without peptide. Mixtures were allowed to equilibrate for 5 min at room temperature, enzymatic reactions were initiated by addition of acetyl-CoA (50 μM final concentration) and incubated for 20 min at 37 °C. Upon completion, reactions were stopped with 1:1 volume of cold isopropanol and CPM (7-diethylamino-3-(4′-maleimidylphenyl)-4-methylcoumarin, 12.5 μM final concentration). After incubation for 15 min at room temperature, plates were read in a fluorescence microplate reader (POLARStar OPTIMA, BMG Labtech) at Ex = 390 nm/Em = 460 nm with a gain setting of 1391. For competition analysis, concentrations of acetyl-CoA or histone H3 peptide were varied over 0.78–50 μM and 3.1–200 μM, respectively. Standard curves were generated by preparing a twofold dilution series of freshly dissolved acetyl-CoA in assay buffer covering a concentration range of 0–50 μM. Samples were then mixed with isopropanol, reacted with CPM, and measured as described above.

SDS-PAGE and immunoblotting
HEK293T cells were treated with NDGA for 24 h and lysed in lysis buffer (20 mM Tris-HCl pH 7.5, 150 mM NaCl, 1 mM Na₂EDTA, and 1 mM EGTA, 1% TritonX100) supplemented with complete EDTA-free protease inhibitor cocktail (ROCHE) and PhosStop phosphatase inhibitor cocktail (ROCHE). Polyacrylamide gels (10–15%) were used for the separation of total proteins. Thirty micrograms of total proteins were transferred to 0.2 μm nitrocellulose membranes using the BioRad blotting system. Histones were extracted from HEK293T cells by EpiQuik Total Histone Extraction Kit (Epigentek), following manufacturer's instructions. One to five micrograms of histone isolates was separated by Polyacrylamide gels (15%) and transferred to 0.5-μm nitrocellulose membranes using the BioRad blotting system. All membranes were blocked with blocking buffer (5% BSA in TBST) and probed with primary and then secondary antibody. Antibodies used are shown in Supplementary Notes. Lumi-Light Western Blotting Substrate (ROCHE) or SuperSignal West Femto Maximum Sensitivity Substrate (Thermo Fisher) were used for detection of the target proteins. Chemiluminescence intensities were detected using the ChemiDoc imaging system (BioRad) and quantified using Image J software (NIH). β-actin levels were used to normalize the intensities of bands. For CETSA curves, the band intensities were related to the intensities of the lowest temperature for the control samples or drug-exposed sample. For the ITDRF_CETSA experiments, the band intensities were related to control samples. All experiments were performed at least twice. All blots derive from the same experiment and were processed in parallel.

Cellular thermal shift assay (CETSA)
For CETSA, HEK293T cells were freshly seeded the day before the experiment. The day of experiment, equal numbers of cells were counted by Moxi Mini automated cell counter (Orflo), and 0.6×10^6 cells per temperature were seeded in T-25 cell culture flasks (VWR) in an appropriate volume of culture medium. Cells were exposed to 100 μM NDGA or equal volume DMSO for 3 h in an incubator with 5% CO₂ and 37 °C. After the incubation, cells were harvested, washed with PBS, and resuspended in PBS supplemented with EDTA-free complete protease inhibitor cocktail (ROCHE). Intact cells were divided into 100-μl aliquots and heated individually at different temperatures for 3 min in a PCR machine (Thermal cycler, BIO-RAD), followed by cooling for 2 min at room temperature. Cell suspensions were freeze-thawed three times using liquid nitrogen, and the soluble fraction was separated from the cell debris by centrifugation at 20,000×g for 20 min at 4 °C. Supernatants were transferred to new micro centrifuge tubes and analyzed by SDS-PAGE, followed by immunoblotting analysis. Immunoblotting results were subjected to densitometry analysis (ImageJ, NIH), and melting temperatures of p300-HAT, PCAF, GCN5, and TIP60 were determined by Prism 7 software (GraphPad) using nonlinear regression fit. The viability of the cells was assessed in triplicate by trypan

blue exclusion. All CETSA experiments were performed at least as triplicates.

Isothermal dose response fingerprint-cellular thermal shift assay (ITDRF$_{CETSA}$)

HEK293T cells were treated with different concentrations of NDGA and prepared as described above. Intact cells were aliquoted (0.6×10^6 cells per concentration) into PCR tubes and heated at 55 °C, where 35% of p300 HAT protein remained in the soluble fraction) for 3 min. Samples were cooled down for an additional 2 min at room temperature and freeze-thawed three times using liquid nitrogen. The soluble fraction was separated by centrifugation at $20,000 \times g$ for 20 min at 4 °C and subjected to immunoblotting. ITDRF$_{CETSA}$ experiments were performed at least as triplicates.

Flow cytometry

HeLa GFP-LC3 cells were analyzed by FACS as described.[67] Briefly, cells were collected by trypsin and washed with cold PBS. The pellets were resuspended with 0.05% Saponin (diluted in PBS), vortexed briefly and added six volumes of PBS to further dilute the detergent. Cells were pelleted, resuspended with PBS and monitored by FACS (BD Bioscience). Results were analyzed by FACSDiva 8.0.2 software.

Confocal microscopy

GFP-LC3 HeLa cells were seeded onto glass slide-chamber (Watson Bio Lab) and treated with NDGA (30 μM) for 24 h and prepared for confocal microscopy. Cells were fixed with 1.6% paraformaldehyde (Alfa Aesar) for 15 min at RT and washed with PBS. Then, to stain nuclei, GFP-LC3 HeLa cells were incubated with DAPI (Genetex) for 5 min at RT. After three PBS washes, slides were prepared with mounting solution Tris-MWL 4-88 (Citifluor) for imaging. Samples were viewed on a temperature controlled Zeiss 780 LSM confocal fluorescent microscope (488 nm for GFP, 405 nm for DAPI, ×63/1.4 oil-immersion objective) in the Buck Institute for Research on Aging Morphology Core. 16-bit images (2048 × 2048, C:2, Z:1, T:1) were analyzed using Zen 2.3 2011 software (Zeiss) and Image J software (NIH). GFP-LC3 puncta-positive cells were quantified using the Image J object counter plug-in. Cells that contained 15 or more puncta per cell were considered LC3-positive, and this threshold value (15 puncta/cell) was used to determine the percentage of autophagic cells as described.[68]

Caenorhabditis elegans maintenance and lifespan assay

C. elegans hermaphrodites were maintained on nematode growth medium (NGM) agar plates seeded with E. coli bacterial strain OP50 at 20 °C as described.[69] Strains used in this study were wildtype Bristol N2 and MAH215 (sqIs11 [lgg-1p::mCherry::GFP::lgg-1 + rol-6] rollers. Wildtype N2 Bristol worms were synchronized by a 2-h egg lay from gravid adult hermaphrodites, and the eggs were transferred to NGM plates containing 100 μM NDGA with a bacterial OP50 lawn at 20 °C. Worms were scored as dead when they no longer responded to gentle prodding with a platinum wire. The lifespan of an individual was defined as the time elapsed from when it was placed onto the fresh NGM plate ($t = 0$) to when it was scored as dead. Nematodes that crawled off plates during the assay were excluded from calculations.

OP50 growth assay

E. coli OP50 culture was grown in LB overnight at 37 °C shaker (200 rpm). The day after, the culture was diluted 1:1000 in LB containing either 100 μM NDGA or the same volume of DMSO. The absorbance at 595 nm was measured by SpectraMax i3X every hour. Experiments were performed in eight technical replicates in a total of three independent experiments and plotted as time-dependent growth curve.

Mounting worms and imaging

NDGA (100 μM) was prepared in sterile water and added to the top of NGM plates seeded with an OP50 lawn. On their first day of adulthood, synchronized population of worms were transferred to either DMSO control or NDGA-treated plates for experimental analysis. Microscopic slides containing pads of 2% agarose (Sigma) were prepared 30 min before mounting worms. Around 2–5 μl of 2 mM levamisole (Sigma) was pipetted

out on the center of the agarose pads. Worms were transferred to the levamisole drop, and a cover slip was placed on top before imaging.

Lysotracker red staining

Synchronized day-1 adult N2 worms were transferred to DMSO control or NDGA-treated plates for 24 h at 20 °C. On day 2, worms were transferred to OP50-seeded plates treated with NDGA and containing 1 μM LysoTracker Red DND-99 (Molecular Probes) for 24 h at 20 °C. After 24 h, worms were picked and washed in a fresh drop of 1X M9 medium and mounted on 2% agarose pad slides for microscopic visualization. Worm images were taken in a Zeiss Imager Z1 fluorescence microscope using rhodamine filters. Image analysis was performed by measuring mean LysoTracker fluorescence of each worm using Image J (NIH) software.

Tandem-tagged LGG-1 reporter imaging

MAH215 worms were synchronized and transferred to DMSO control or NDGA-treated plates on day 1 of adulthood as above. After 2 or 24 h, worms were imaged using GFP and rhodamine filters on a Zeiss fluorescence microscope. For each worm, we quantified the number of mCherry-only puncta (i.e., autolysosmes (AL) (the total number of mCherry-positive punctae − the number of GFP-intensity) as described.

Worm protein extraction

Synchronized day-1 adult N2 worms were transferred to DMSO control or NDGA treated plates for 24 h at 20 °C. One hundred worms from each treatment condition were collected in 1X M9 solution. Worms were washed twice and suspended in RIPA lysis buffer. Worm pellets were sonicated for 10 cycles at maximum intensity in Bioruptor sonicator (Diagenode). Lysate was centrifuged at $1000 g$ for 1 min, and clear protein lysate was used for immunoblotting.

Statistical analysis

Dose-response analysis of histone acetylation in cells was analyzed by nonlinear regression fit to $Y = 100/(1 + 10 (\text{Log IC50} - X)*H)$, where $H = $ Hill slope (variable). IC_{50} values represent the concentration of NDGA that inhibits 50% of the occurrence of acetylation of the target residue. The experiments in which wildtype and mutant p300 plasmids used were subjected to correlation analysis by a Pearson correlation. CETSA data were expressed as means ± SD. Band intensities from independent experiments ($n \geq 2$) were plotted using nonlinear regression fit (variable slope). ITDRF$_{CETSA}$ data were fitted using a sigmoidal (variable slope) curve fit. Multiple confocal microscopy images ($n \geq 100$ cells per condition) were analyzed, and data were expressed as means ± SD. P values were determined by unpaired, two-tailed Student's t tests. (*$p < 0.05$; **$p < 0.01$; ***$p < 0.001$; ****$p < 0.0001$). P values in lifespan curves were calculated using the log-rank (Mantel–Cox) test. In the tandem-tagged LGG-1 reporter imaging, the average puncta were calculated, and data were analyzed using one-way analysis of variance ANOVA. All calculations were performed using Prism 7 (GraphPad) software.

Reporting summary

Further information on research design is available in the Nature Research Reporting Summary linked to this article.

REFERENCES

1. Lopez-Otin, C., Blasco, M. A., Partridge, L., Serrano, M. & Kroemer, G. The hallmarks of aging. Cell **153**, 1194–1217 (2013).
2. de Cabo, R., Carmona-Gutierrez, D., Bernier, M., Hall, M. N. & Madeo, F. The search for antiaging interventions: from elixirs to fasting regimens. Cell **157**, 1515–1526 (2014).

3. Harrison, D. E. et al. Rapamycin fed late in life extends lifespan in genetically heterogeneous mice. *Nature* **460**, 392–395 (2009).

4. Strong, R. et al. Nordihydroguaiaretic acid and aspirin increase lifespan of genetically heterogeneous male mice. *Aging Cell* **7**, 641–650 (2008).

5. Harrison, D. E. et al. Acarbose, 17-alpha-estradiol, and nordihydroguaiaretic acid extend mouse lifespan preferentially in males. *Aging Cell* **13**, 273–282 (2014).

6. Strong, R. et al. Longer lifespan in male mice treated with a weakly estrogenic agonist, an antioxidant, an alpha-glucosidase inhibitor or a Nrf2-inducer. *Aging Cell* **15**, 872–884 (2016).

7. Economos, A. C., Ballard, R. C., Miquel, J., Binnard, R. & Philpott, D. E. Accelerated aging of fasted Drosophila. Preservation of physiological function and cellular fine structure by thiazolidine carboxylic acid (TCA). *Exp. Gerontol.* **17**, 105–114 (1982).

8. Richie, J. P., Jr. Mills, B. J. & Lang, C. A. Dietary nordihydroguaiaretic acid increases the life span of the mosquito. *Proc. Soc. Exp. Biol. Med* **183**, 81–85 (1986).

9. Siddique, Y. H., Ara, G., Jyoti, S. & Afzal, M. The dietary supplementation of nordihydroguaiaretic acid (NDGA) delayed the loss of climbing ability in Drosophila model of Parkinson's disease. *J. Diet. Suppl.* **9**, 1–8 (2012).

10. West, M. et al. The arachidonic acid 5-lipoxygenase inhibitor nordihydroguaiaretic acid inhibits tumor necrosis factor alpha activation of microglia and extends survival of G93A-SOD1 transgenic mice. *J. Neurochem.* **91**, 133–143 (2004).

11. Lee, J. et al. Modulation of lipid peroxidation and mitochondrial function improves neuropathology in Huntington's disease mice. *Acta Neuropathol.* **121**, 487–498 (2011).

12. Hamaguchi, T., Ono, K., Murase, A. & Yamada, M. Phenolic compounds prevent Alzheimer's pathology through different effects on the amyloid-beta aggregation pathway. *Am. J. Pathol.* **175**, 2557–2565 (2009).

13. Goodman, Y., Steiner, M. R., Steiner, S. M. & Mattson, M. P. Nordihydroguaiaretic acid protects hippocampal neurons against amyloid beta-peptide toxicity, and attenuates free radical and calcium accumulation. *Brain Res.* **654**, 171–176 (1994).

14. Floriano-Sanchez, E. et al. Nordihydroguaiaretic acid is a potent in vitro scavenger of peroxynitrite, singlet oxygen, hydroxyl radical, superoxide anion and hypochlorous acid and prevents in vivo ozone-induced tyrosine nitration in lungs. *Free Radic. Res.* **40**, 523–533 (2006).

15. Arteaga, S., Andrade-Cetto, A. & Cardenas, R. Larrea tridentata (Creosote bush), an abundant plant of Mexican and US-American deserts and its metabolite nordihydroguaiaretic acid. *J. Ethnopharmacol.* **98**, 231–239 (2005).

16. Rojo, A. I. et al. Signaling pathways activated by the phytochemical nordihydroguaiaretic acid contribute to a Keap1-independent regulation of Nrf2 stability: role of glycogen synthase kinase-3. *Free Radic. Biol. Med.* **52**, 473–487 (2012).

17. Peleg, S., Feller, C., Ladurner, A. G. & Imhof, A. The metabolic impact on histone acetylation and transcription in ageing. *Trends Biochem. Sci.* **41**, 700–711 (2016).

18. Gelino, S. & Hansen, M. Autophagy—an emerging anti-aging mechanism. *J. Clin. Exp. Pathol.* **Suppl 4**, pii: 006 (2012).

19. Eisenberg, T. et al. Nucleocytosolic depletion of the energy metabolite acetyl-coenzyme a stimulates autophagy and prolongs lifespan. *Cell Metab.* **19**, 431–444 (2014).

20. Pietrocola, F., Galluzzi, L., Bravo-San Pedro, J. M., Madeo, F. & Kroemer, G. Acetyl coenzyme A: a central metabolite and second messenger. *Cell Metab.* **21**, 805–821 (2015).

21. Simon, R. P., Robaa, D., Alhalabi, Z., Sippl, W. & Jung, M. KATching-up on small molecule modulators of lysine acetyltransferases. *J. Med. Chem.* **59**, 1249–1270 (2016).

22. Sebti, S. et al. BAT3 modulates p300-dependent acetylation of p53 and autophagy-related protein 7 (ATG7) during autophagy. *Proc. Natl Acad. Sci. USA* **111**, 4115–4120 (2014).

23. Marino, G. et al. Regulation of autophagy by cytosolic acetyl-coenzyme A. *Mol. Cell* **53**, 710–725 (2014).

24. Lee, I. H. & Finkel, T. Regulation of autophagy by the p300 acetyltransferase. *J. Biol. Chem.* **284**, 6322–6328 (2009).

25. Salari, H., Braquet, P. & Borgeat, P. Comparative effects of indomethacin, acetylenic acids, 15-HETE, nordihydroguaiaretic acid and BW755C on the metabolism of arachidonic acid in human leukocytes and platelets. *Prostaglandins Leukot. Med.* **13**, 53–60 (1984).

26. Hurst, J. S. & Bazan, H. E. The sensitivity of bovine corneal epithelial lyso-PAF acetyltransferase to cyclooxygenase and lipoxygenase inhibitors is independent of arachidonate metabolites. *J. Ocul. Pharm. Ther.* **13**, 415–426 (1997).

27. White, H. L. & Faison, L. D. Inhibition of lyso-PAF: acetyl-CoA acetyltransferase by salicylates and other compounds. *Prostaglandins* **35**, 939–944 (1988).

28. Shirakawa, K. et al. Salicylate, diflunisal and their metabolites inhibit CBP/p300 and exhibit anticancer activity. *Elife* **5**, https://doi.org/10.7554/eLife.11156 (2016).

29. Dancy, B. M. & Cole, P. A. Protein lysine acetylation by p300/CBP. *Chem. Rev.* **115**, 2419–2452 (2015).

30. Thompson, P. R. et al. Regulation of the p300 HAT domain via a novel activation loop. *Nat. Struct. Mol. Biol.* **11**, 308–315 (2004).

31. Balasubramanyam, K., Swaminathan, V., Ranganathan, A. & Kundu, T. K. Small molecule modulators of histone acetyltransferase p300. *J. Biol. Chem.* **278**, 19134–19140 (2003).

32. Ogryzko, V. V., Schiltz, R. L., Russanova, V., Howard, B. H. & Nakatani, Y. The transcriptional coactivators p300 and CBP are histone acetyltransferases. *Cell* **87**, 953–959 (1996).

33. Jin, Q. et al. Distinct roles of GCN5/PCAF-mediated H3K9ac and CBP/p300-mediated H3K18/27ac in nuclear receptor transactivation. *EMBO J.* **30**, 249–262 (2011).

34. McCauley, B. S. & Dang, W. Histone methylation and aging: lessons learned from model systems. *Biochim. Biophys. Acta* **1839**, 1454–1462 (2014).

35. McCord, R. P. et al. Correlated alterations in genome organization, histone methylation, and DNA-lamin A/C interactions in Hutchinson-Gilford progeria syndrome. *Genome Res.* **23**, 260–269 (2013).

36. Buffenstein, R. The naked mole-rat: a new long-living model for human aging research. *J. Gerontol. A Biol. Sci. Med. Sci.* **60**, 1369–1377 (2005).

37. Tan, L. et al. Naked mole rat cells have a stable epigenome that resists iPSC reprogramming. *Stem Cell Rep.* **9**, 1721–1734 (2017).

38. Crump, N. T. et al. Dynamic acetylation of all lysine-4 trimethylated histone H3 is evolutionarily conserved and mediated by p300/CBP. *Proc. Natl Acad. Sci. USA* **108**, 7814–7819 (2011).

39. Suzuki, T., Kimura, A., Nagai, R. & Horikoshi, M. Regulation of interaction of the acetyltransferase region of p300 and the DNA-binding domain of Sp1 on and through DNA binding. *Genes Cells* **5**, 29–41 (2000).

40. Martinez Molina, D. et al. Monitoring drug target engagement in cells and tissues using the cellular thermal shift assay. *Science* **341**, 84–87 (2013).

41. Levine, B. & Kroemer, G. Autophagy in the pathogenesis of disease. *Cell* **132**, 27–42 (2008).

42. Hansen, M., Rubinsztein, D. C. & Walker, D. W. Autophagy as a promoter of longevity: insights from model organisms. *Nat. Rev. Mol. Cell Biol.* **19**, 579–593 (2018).

43. Rubinsztein, D. C., Shpilka, T. & Elazar, Z. Mechanisms of autophagosome biogenesis. *Curr. Biol.* **22**, R29–R34 (2012).

44. Yoshimori, T., Yamamoto, A., Moriyama, Y., Futai, M. & Tashiro, Y. Bafilomycin A1, a specific inhibitor of vacuolar-type H(+)-ATPase, inhibits acidification and protein degradation in lysosomes of cultured cells. *J. Biol. Chem.* **266**, 17707–17712 (1991).

45. Seglen, P. O., Grinde, B. & Solheim, A. E. Inhibition of the lysosomal pathway of protein degradation in isolated rat hepatocytes by ammonia, methylamine, chloroquine and leupeptin. *Eur. J. Biochem.* **95**, 215–225 (1979).

46. Victor, M. et al. HAT activity is essential for CBP-1-dependent transcription and differentiation in Caenorhabditis elegans. *EMBO Rep.* **3**, 50–55 (2002).

47. Chang, J. T., Kumsta, C., Hellman, A. B., Adams, L. M. & Hansen, M. Spatiotemporal regulation of autophagy during Caenorhabditis elegans aging. *Elife* **6**, https://doi.org/10.7554/eLife.18459 (2017).

48. Akimaru, H. et al. Drosophila CBP is a co-activator of cubitus interruptus in hedgehog signalling. *Nature* **386**, 735–738 (1997).

49. Yao, T. P. et al. Gene dosage-dependent embryonic development and proliferation defects in mice lacking the transcriptional integrator p300. *Cell* **93**, 361–372 (1998).

50. Farria, A., Li, W. & Dent, S. Y. KATs in cancer: functions and therapies. *Oncogene* **34**, 4901–4913 (2015).

51. Valor, L. M., Viosca, J., Lopez-Atalaya, J. P. & Barco, A. Lysine acetyltransferases CBP and p300 as therapeutic targets in cognitive and neurodegenerative disorders. *Curr. Pharm. Des.* **19**, 5051–5064 (2013).

52. Brown, J. A., Bourke, E., Eriksson, L. A. & Kerin, M. J. Targeting cancer using KAT inhibitors to mimic lethal knockouts. *Biochem. Soc. Trans.* **44**, 979–986 (2016).

53. Gaddis, M., Gerrard, D., Frietze, S. & Farnham, P. J. Altering cancer transcriptomes using epigenomic inhibitors. *Epigenetics Chromatin* **8**, 9 (2015).

54. Lasko, L. M. et al. Discovery of a selective catalytic p300/CBP inhibitor that targets lineage-specific tumours. *Nature* **550**, 128–132 (2017).

55. Lafuente-Lafuente, C. et al. Amiodarone concentrations in plasma and fat tissue during chronic treatment and related toxicity. *Br. J. Clin. Pharm.* **67**, 511–519 (2009).

56. Damle, B., Stogniew, M. & Dowell, J. Pharmacokinetics and tissue distribution of anidulafungin in rats. *Antimicrob. Agents Chemother.* **52**, 2673–2676 (2008).

57. Jenny, N. S. Inflammation in aging: cause, effect, or both? *Disco. Med.* **13**, 451–460 (2012).

58. Congdon, E. E. Sex differences in autophagy contribute to female vulnerability in Alzheimer's disease. *Front. Neurosci.* **12**, 372 (2018).

59. Rubinsztein, D. C., Marino, G. & Kroemer, G. Autophagy and aging. *Cell* **146**, 682–695 (2011).

60. Madeo, F., Zimmermann, A., Maiuri, M. C. & Kroemer, G. Essential role for autophagy in life span extension. *J. Clin. Investig.* **125**, 85–93 (2015).

61. Eisenberg, T. et al. Induction of autophagy by spermidine promotes longevity. *Nat. Cell Biol.* **11**, 1305–1314 (2009).

62. Mercken, E. M. et al. SIRT1 but not its increased expression is essential for lifespan extension in caloric-restricted mice. *Aging Cell* **13**, 193–196 (2014).
63. Pietrocola, F. et al. Aspirin recapitulates features of caloric restriction. *Cell Rep.* **22**, 2395–2407 (2018).
64. Bjedov, I. et al. Mechanisms of life span extension by rapamycin in the fruit fly Drosophila melanogaster. *Cell Metab.* **11**, 35–46 (2010).
65. Castoldi, F., Pietrocola, F., Maiuri, M. C. & Kroemer, G. Aspirin induces autophagy via inhibition of the acetyltransferase EP300. *Oncotarget* **9**, 24574–24575 (2018).
66. Wan, W. et al. mTORC1 phosphorylates acetyltransferase p300 to regulate autophagy and lipogenesis. *Mol. Cell* **68**, 323–335 e326 (2017).
67. Eng, K. E., Panas, M. D., Karlsson Hedestam, G. B. & McInerney, G. M. A novel quantitative flow cytometry-based assay for autophagy. *Autophagy* **6**, 634–641 (2010).
68. Klionsky, D. J. et al. Guidelines for the use and interpretation of assays for monitoring autophagy (3rd edition). *Autophagy* **12**, 1–222 (2016).
69. Brenner, S. The genetics of Caenorhabditis elegans. *Genetics* **77**, 71–94 (1974).

ACKNOWLEDGEMENTS

AUTHOR CONTRIBUTIONS

T.T. designed and performed experiments, analyzed data, and wrote the manuscript. C.N. performed in vitro studies in Fig. 1a, b and was responsible from the provision of study materials; R.P.S. conducted assays in Fig. 1c–f with the supervision of M.J.; M.C. conducted assays in Fig. 5e–i with the supervision of J.A.; T.T. conducted assays in Fig. 5a, b together with V.J.B. under the supervision of A.W.K.; E.V. supervised the study and edited the manuscript. All authors discussed the results and contributed to the final manuscript.

COMPETING INTERESTS

The authors declare no competing interests.

ADDITIONAL INFORMATION

Supplementary information is available for this paper at https://doi.org/10.1038/s41514-019-0037-7.

Correspondence and requests for materials should be addressed to E.V.

Reprints and permission information is available at http://www.nature.com/reprints

Publisher's note Springer Nature remains neutral with regard to jurisdictional claims in published maps and institutional affiliations.